

Article

Facile Electrodeposition of Poly(3,4-ethylenedioxythiophene) on Poly(vinyl alcohol) Nanofibers as the Positive Electrode for High-Performance Asymmetric Supercapacitor

Nivekthiren Dasdevan ¹, Muhammad Amirul Aizat Mohd Abdah ¹ and Yusran Sulaiman ^{1,2,*} 

¹ Department of Chemistry, Faculty of Science, Universiti Putra Malaysia, UPM Serdang 43400, Selangor, Malaysia

² Functional Devices Laboratory, Institute of Advanced Technology, Universiti Putra Malaysia, UPM Serdang 43400, Selangor, Malaysia

* Correspondence: yusran@upm.edu.my

Received: 19 June 2019; Accepted: 17 July 2019; Published: 2 September 2019



Abstract: Poly(vinyl alcohol)/poly(3,4-ethylenedioxythiophene) (PVA/PEDOT) nanofibers were synthesized as a positive electrode for high-performance asymmetric supercapacitor (ASC). PVA/PEDOT nanofibers were prepared through electrospinning and electrodeposition meanwhile reduced graphene oxide (rGO) was obtained by electrochemical reduction. The PVA/PEDOT nanofibers demonstrated cauliflower-like morphology showing that PEDOT was uniformly coated on the smooth cross-linking structure of PVA nanofibers. In addition, the ASC showed a remarkable energy output efficiency by delivering specific energy of 21.45 Wh·kg⁻¹ at a specific power of 335.50 W·kg⁻¹ with good cyclability performance (83% capacitance retained) after 5000 CV cycles. The outstanding supercapacitive performance is contributed from the synergistic effects of both PVA/PEDOT//rGO, which gives promising materials for designing high-performance supercapacitor applications.

Keywords: asymmetric supercapacitor; nanofiber; reduced graphene oxide; potential window

1. Introduction

Electrochemical energy storage devices, such as fuel cells, batteries, and supercapacitors, apply the principle of chemical-to-electrical energy conversion [1]. Supercapacitors possess significant advantages compared to other energy storages due to its fast charging and discharging, long cycle life, low cost and good environmental friendliness [2]. Supercapacitors bridging the energy storage gap between batteries and conventional capacitors and widely being used for hybrid electric vehicles, medical applications, military, and diesel locomotives [3,4]. However, high specific power, long cycle life time and portability of supercapacitors make it more demand than batteries [5]. The energy storage mechanism of a supercapacitor can be classified into the electrical double-layer capacitor (EDLC) and pseudocapacitors [6,7]. EDLCs (carbon-based electrode materials) store charges via ion accumulation at the interface of carbon-based electrodes [8] which has high specific power [9], large specific surface area and controllable pore-characteristics for high cycling stability [10,11]. Unfortunately, it suffers from low specific capacitance and specific energy which can affect the performance of supercapacitors [10]. Pseudocapacitors (transition metal oxide and conducting polymer) undergo highly reversible redox reactions taking place on the surface or near the electrodes [12] and able to deliver a higher specific capacitance and specific energy than EDLC because they have different oxidation states for rich redox reactions [13].

An asymmetric supercapacitor (ASC) consists of EDLC (power source) and pseudocapacitor (energy source) as negative and positive electrodes, respectively [10] where both electrodes have

different charge storage mechanism and well separated potential windows are assembled in the same electrolyte [14]. Thus, it exhibits a wide potential window which leads to higher specific energy and specific power for asymmetric supercapacitors [14].

Reduced graphene oxide (rGO) can be prepared from graphene oxide (GO) through chemical, electrochemical, thermal, hydrothermal, and photocatalytic routes. Among these methods, electrochemical reduction of GO is easy, cheap, fast and environmentally friendly to yield the bulk amount of graphene material. Jiang et al. [15] reported that nickel foam-reduced graphene oxide/nickel-cobalt layered doubled layered hydroxide/nickel foam-reduced graphene oxide (NF-rGO/Ni-Co LDH/NF-rGO) displayed outstanding gravimetric capacitance of $1454.2 \text{ F}\cdot\text{g}^{-1}$ at 1 A g^{-1} in 1 M KOH electrolyte. In addition, asymmetric Ni-Co-O-rGO//AC possessed $1903 \text{ F}\cdot\text{g}^{-1}$ of specific capacitance using KOH/redox active $\text{K}_3\text{Fe}(\text{CN})_6$ as electrolyte [16]. Huang et al. [17] fabricated LDH/rGO-4//rGO composite via solvothermal approach and exhibited specific energy of $29.3 \text{ Wh}\cdot\text{kg}^{-1}$ and the capacitance can be retained from $82.5 \text{ F}\cdot\text{g}^{-1}$ to $21.9 \text{ F}\cdot\text{g}^{-1}$ at a current density between 0.5 A g^{-1} to 7 A g^{-1} , proving its good rate capability.

Poly(3,4-ethylenedioxythiophene) (PEDOT) is used as a pseudocapacitive electrode in asymmetric supercapacitors due to its high conductivity, excellent processability and economic [18]. In addition, PEDOT is available in both an oxidized state and reduced state. Yang et al. [19] revealed that NiO/Ni(OH)₂/PEDOT electrodes could deliver $80.8 \text{ F}\cdot\text{cm}^{-3}$ of specific capacitance. An ASC of PEDOT//activated carbon (AC) obtained a specific capacitance of $22 \text{ F}\cdot\text{g}^{-1}$ and $27 \text{ F}\cdot\text{g}^{-1}$ in $1 \text{ M Et}_4\text{NBF}_4$ /propylene carbonate and LiPF_6 /ethylene carbonate/dimethyl carbonate, respectively [20].

Recently, the usage of electrospinning technique has been widely explored for preparing nanofiber membranes in ASC devices due to its facile preparation and economical. For example, manganese oxide/porous carbon nanofibers//activated carbon (MnO_2 /PCNF_s/AC) was fabricated via electrospinning and subsequent chemical precipitation approach and exhibited a specific capacitance of $60.6 \text{ F}\cdot\text{g}^{-1}$ [21]. High specific energy of $15.0 \text{ Wh}\cdot\text{kg}^{-1}$ was achieved by the assembled ASC of cobalt sulfides/carbon//porous carbon nanofibers (CoS_x /C//PCNF_s) which was fabricated using electrospinning and hydrothermal routes [22]. Hollow carbon nanofibers (HCNF_s) coated with MnO_2 (HCNF_s/HCNF_s) which were assembled with PCNF_s in a coin cell set up producing a gravimetric capacitance of $63.9 \text{ F}\cdot\text{g}^{-1}$ with an extended operating voltage up to 2.0 V [23]. Production of PVA nanofibers has attracted a lot of attention owing to its excellent mechanical properties, good adherence properties towards porous and water surfaces and environmental friendly [24,25]. PVA is one of the biodegradable polymers that has been used as a precursor to produce electrospun nanofibers. The abundance of hydrophilic functional groups (–OH) on the PVA structure makes them highly soluble in an aqueous medium. Pan et al. [26] have synthesized PVA-GO electrospun nanofibers which act as a separator via drop casting and laser-writing process for solid-state supercapacitors. The porous architecture of PVA-GO nanofibers and hygroscopic feature of GO could effectively improve the electrolyte uptake during charging/discharging process. The solid-state supercapacitor using PVA-GO nanofibers also showed high areal capacitance ($9.9 \text{ mF}\cdot\text{cm}^{-2}$), remarkable specific energy ($0.13 \text{ mW}\cdot\text{cm}^{-3}$) and excellent cycling stability (88% capacitance retained after 1000 cycles). However, PVA nanofibers are non-conductive materials which need to be incorporated with a conductive material such as PEDOT in order to overcome the drawback. Therefore, the combination of PVA nanofiber and PEDOT could synergistically improve the electrochemical behavior of the positive electrode. Inspired by this idea, high-performance asymmetric supercapacitor was fabricated using PVA/PEDOT nanofibers and rGO as a positive and negative electrode, respectively, with different potential windows to increase the overall voltage of asymmetric supercapacitor. The extended potential windows and synergistic effect of high capacitance, good conductivity and outstanding cycling stability of PVA/PEDOT//rGO can deliver excellent capacitive performance of ASC device, implying a promising material for future supercapacitor application.

2. Materials and Methods

2.1. Materials

Indium tin oxide (ITO) glasses were obtained from Xin Yan Technology. Polyvinyl alcohol (PVA), lithium perchlorate (LiClO_4), sodium chloride (NaCl) and 3,4-ethylenedioxythiophene (EDOT) were supplied by Sigma Aldrich. GO was obtained from Graphenea. Ethanol and potassium chloride (KCl) were purchased from HmbG Chemicals and Fisher Scientific UK, respectively. Acetone was supplied by System. Acetonitrile and hydrochloric acid were obtained from J.T Baker. Deionized water ($18.2 \text{ M}\Omega\cdot\text{cm}$) was used throughout the experiment.

2.2. Preparation of PVA Nanofiber via Electrospinning

ITO glasses (1 cm^2) were cleaned with acetone followed by ethanol and deionized water for 10 min using a sonicator bath. PVA solution (10 wt%, 0.4 g) was prepared and heated at $80 \text{ }^\circ\text{C}$ and continuously stirred for 30 min until a clear solution was observed. The PVA solution was transferred into a 5-mL syringe and connected to the syringe pump. The collector plate was covered with aluminum foil and ITO glasses were attached on the plate surface. 15 kV of voltage was applied directly to the stainless-steel needle. The operating flow rate of solution and the distance from the syringe nozzle to the collector were controlled to $1.2 \text{ mL}\cdot\text{h}^{-1}$ and 15 cm, respectively.

2.3. Electrodeposition of PEDOT on PVA Nanofibers

A non-aqueous EDOT solution which consists of 0.01 M EDOT and 0.1 M LiClO_4 in acetonitrile was prepared. Chronoamperometry (CA) was used to perform electrodeposition of PEDOT on PVA nanofibers using a three-electrode system at 1.2 V for 15 min. ITO substrate coated with PVA nanofibers was used as a working electrode, silver wire coated with silver chloride (Ag/AgCl) as a pseudo-reference electrode and a platinum wire as a counter electrode.

2.4. Reduction of GO

A few drops of $1.0 \text{ mg}\cdot\text{mL}^{-1}$ GO were deposited onto the ITO substrate (1 cm^2) through drop-casting and dried out to form a GO-coated electrode. Electrochemical reduction of the GO-coated electrode was carried out using cyclic voltammetry (CV) in 0.5 M NaCl electrolyte between -1.5 to 0 V for 20 cycles.

2.5. Characterizations

The surface morphologies of the samples were performed using a field emission scanning electron microscope (FESEM, JEOL JSM-7600F). Fourier transform infrared spectroscopy (FTIR) was observed using a Shimadzu. The ASC spectra were analyzed in the range of $400\text{--}4000 \text{ cm}^{-1}$. The electrochemical properties of PVA/PEDOT nanofibers//rGO were characterized by assembling a two-electrode configuration with a piece of filter paper as separator soaked with 1.0 M KCl . CV was conducted between 0 to 1.6 V at scanning rates from $5 \text{ mV}\cdot\text{s}^{-1}$ to $100 \text{ mV}\cdot\text{s}^{-1}$. Galvanostatic charge-discharge (GCD) measurements were performed at different current densities of 0.4 to 0.9 Ag^{-1} . Electrochemical impedance spectroscopy (EIS) tests were carried at open circuit potentials with an amplitude of 5 mV and frequency ranging from 0.01 Hz to 100 kHz. The stability test was examined for 2000 cycles between 0 and 1.6 V. Figure 1 shows the schematic illustration of ASC design based on PVA/PEDOT nanofibers and rGO electrodes. The mass loading of PVA/PEDOT nanofibers//rGO was approximately $0.6 \text{ mg}\cdot\text{cm}^{-2}$.

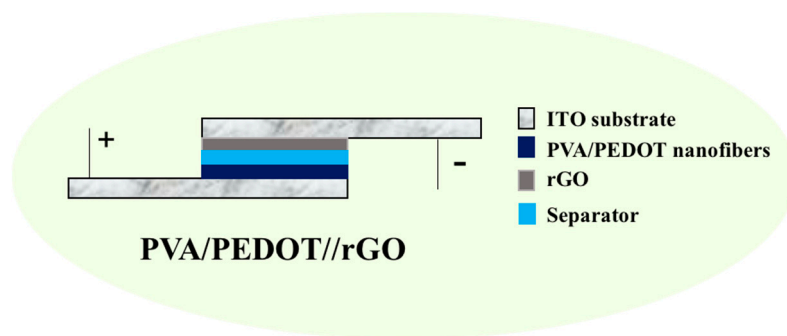


Figure 1. Schematic illustration of asymmetric supercapacitor (ASC) device consisting of the poly(vinyl alcohol)/poly(3,4-ethylenedioxythiophene) (PVA/PEDOT) nanofibers (positive electrode), separator and reduced graphene oxide (rGO) (negative electrode).

3. Results and Discussion

3.1. Structural Morphology

Figure 2 displays the FESEM images of PVA nanofibers, PVA/PEDOT nanofibers and rGO. A smooth cross-linked network structure of PVA nanofibers (Figure 2a) was observed with an average diameter of 72.65 ± 22 nm and beads-free, demonstrating better electrospinnability. The cauliflower-like morphology of PVA/PEDOT nanofibers (Figure 2b) reveals that PEDOT was uniformly coated on the cross-linking morphology of PVA nanofibers without interfering the fibril-like structure of nanofibers [27]. Figure 2c represents the FESEM image of rGO which suggests the wrinkled and crumpled morphology can facilitate rapid ion diffusion and charge transfer at the electrode material [14,28].

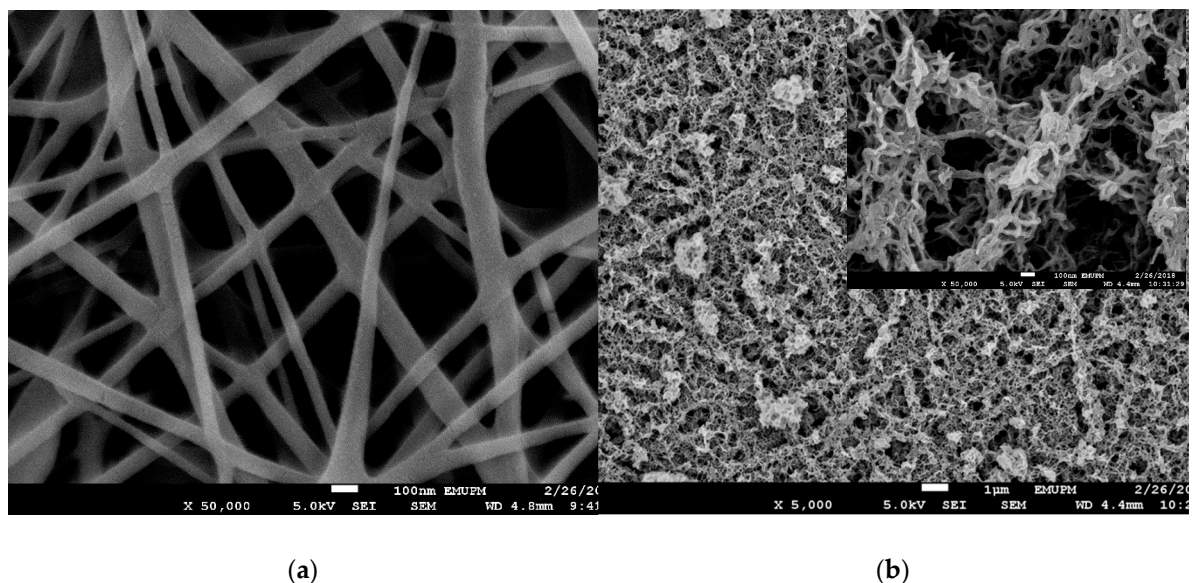
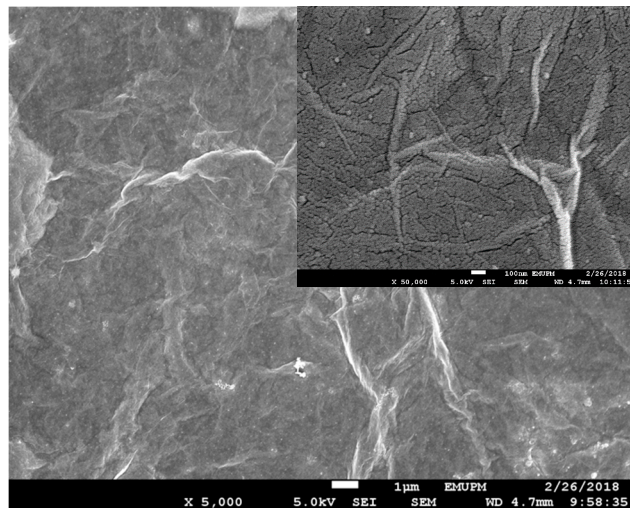


Figure 2. Cont.



(c)

Figure 2. Field emission scanning electron microscope (FESEM) images of (a) PVA nanofibers, (b) PVA/PEDOT nanofibers and (c) rGO. Inset: high magnification of (b) PVA/PEDOT nanofibers and (c) rGO.

3.2. Fourier Transform Infrared Spectroscopy (FTIR)

Fourier transform infrared spectroscopy (FTIR) was employed to identify the functional groups and bonding configuration present [17] in PVA nanofibers, PVA/PEDOT nanofibers, GO and rGO. The FTIR spectrum of PVA nanofibers as depicted in Figure 3 shows the existence of symmetric stretching of C–H and stretching band of C–O group at absorption bands 2906 cm^{-1} and 1087 cm^{-1} , respectively [27]. The broad peak observed at 3284 cm^{-1} and peak at 1438 cm^{-1} are attributed to hydroxyl (O–H) group and C–OH stretching vibration in PVA structure, respectively. From the PVA/PEDOT nanofiber spectrum, peaks of PVA nanofibers can still be seen, proving the presence of PVA nanofibers after electrodeposition of PEDOT. Three characteristic peaks of PEDOT are observed at 775 , 1318 and 1602 cm^{-1} , indicating the C=S, C–C [29], C–C [30] stretching band of thiophene ring in PEDOT structure, respectively. In addition, the C–C stretching of the thiophene ring of PEDOT was observed at 1602 cm^{-1} [30]. The FTIR spectrum of GO reveals the presence of C–O epoxide group, C–OH bond, aromatic C=C bending, C=O group in carboxy and carbonyl groups and O–H stretching vibration at 1107 , 1423 , 1616 , 1732 and 3176 cm^{-1} , respectively. It was also observed that the FTIR spectrum of rGO shows less oxygenated functional groups after electrochemical reduction of GO, indicating rGO has been successfully prepared [31,32].

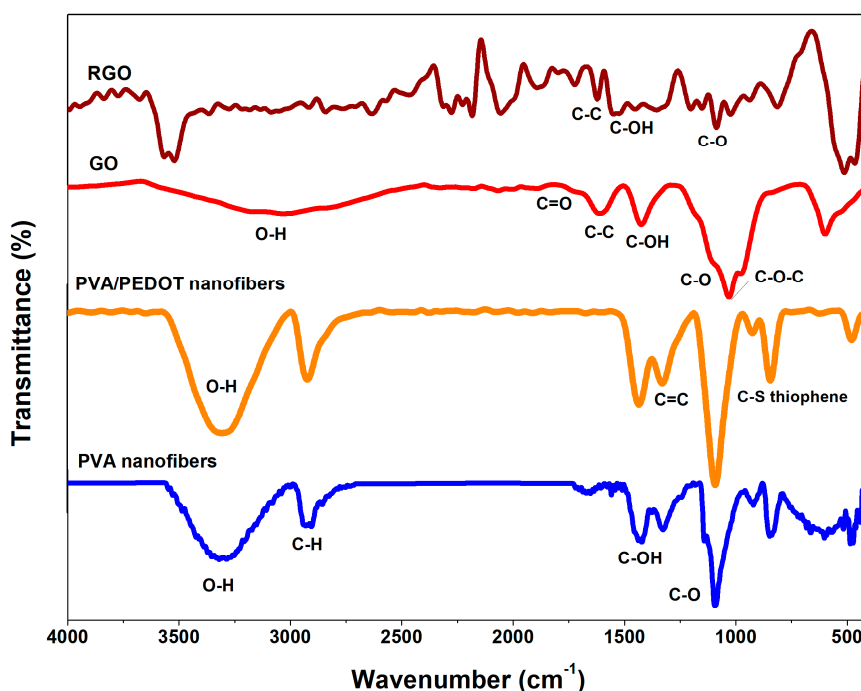


Figure 3. Fourier transform infrared spectroscopy (FTIR) spectra of PVA nanofibers, PVA/PEDOT nanofibers, graphene oxide (GO), and rGO.

3.3. Electrochemical Characterizations

The electrochemical performances of both anode and cathode materials were initially evaluated using a three-electrode system in 1 M KCl electrolyte as shown in Figure 4. Figure 4a display to CV profiles of the individual PEDOT and PVA/PEDOT at a sweeping rate of $25 \text{ mV}\cdot\text{s}^{-1}$ which noted that PVA/PEDOT nanofibers exhibit higher integrated CV area in comparison with PEDOT. This suggests that the formation of PVA nanofibers via electrospinning could provide more accessible sites for electron transfer [33]. The specific capacitance of the ASC is obtained from the CV curve using Equation (1) [10].

$$C = \frac{\int Idv}{vm\Delta V} \quad (1)$$

where C refers to the specific capacitance ($\text{F}\cdot\text{g}^{-1}$), $\int Idv$ is the integrated area of a CV curve, v represents the sweeping rate ($\text{mV}\cdot\text{s}^{-1}$), m is the mass of the electroactive material (g) and ΔV indicates the potential (V). The calculated specific capacitances for PVA/PEDOT, PEDOT and rGO are plotted against scan rates as shown in Figure 4b. The result proves that PVA/PEDOT nanofibers still displays the highest specific capacitance of $331.49 \text{ F}\cdot\text{g}^{-1}$, rather than individual PEDOT ($250.02 \text{ F}\cdot\text{g}^{-1}$) and rGO ($85.92 \text{ F}\cdot\text{g}^{-1}$) at a scan rate of $5 \text{ mV}\cdot\text{s}^{-1}$. However, the rGO electrode shows good rate capability with 83% capacitance retention as compared with PVA/PEDOT (66%) and PEDOT (60%). This indicates that the presence of carbon material could provide good mechanical strength for the remarkable capacitive performance of the electrode [34]. In addition, the electrochemical performance of as-prepared GO and rGO as anode material were also investigated with an applied potential range from -1 to 0 V (Figure 4c). It is obvious that rGO possesses an ideal rectangular CV shape with a higher current response, owing to superior specific capacitance. In Figure 4d, the potential range was measured within -0.2 V to 0.6 V for PVA/PEDOT nanofibers (positive electrode) and -1.0 V to 0 V for RGO (negative electrode) at $25 \text{ mV}\cdot\text{s}^{-1}$. Since both electrodes have different potential windows, the charge storage for both electrodes have to be balanced based on the Equations (2)–(4) [14]:

$$Q_+ = Q_- \quad (2)$$

$$Q = C \times \Delta U \times m \quad (3)$$

$$\frac{m_+}{m_-} = \frac{C_+ \times \Delta U_+}{C_- \times \Delta U_-} \quad (4)$$

where Q_+ and Q_- represent charges stored in the positive electrode and negative electrodes, C_+ and C_- indicate the capacitance for both electrodes, m is the mass loading of electroactive electrode and ΔU represents the potential. A high-performance asymmetric supercapacitor (PVA/PEDOT nanofibers//rGO) of 1.6 V can be constructed based on the sum of potential ranges of two electrodes to further examine the performance of the asymmetric device [35].

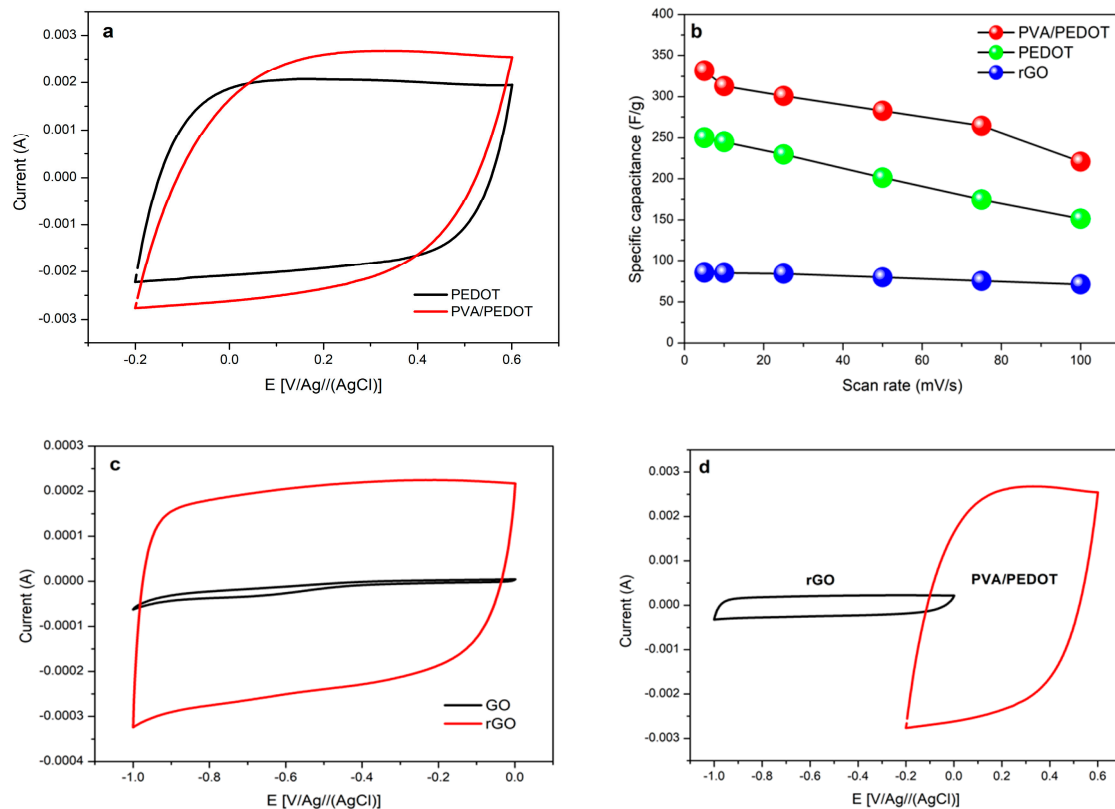


Figure 4. (a) Cyclic voltammety (CV) profiles of PEDOT and PVA/PEDOT at $25 \text{ mV}\cdot\text{s}^{-1}$, (b) Capacitance values of PVA/PEDOT, PEDOT and rGO against sweeping rates ($5\text{--}100 \text{ mV}\cdot\text{s}^{-1}$). (c) CV profiles of GO and rGO at $25 \text{ mV}\cdot\text{s}^{-1}$. (d) CV profiles of rGO and PVA/PEDOT nanofibers measured in a three-electrode configuration in a 1.0 M KCl electrolyte at a sweeping rate of $25 \text{ mV}\cdot\text{s}^{-1}$.

Figure 5a indicates the CV profiles of ASC at various sweeping rates ($5\text{--}100 \text{ mV}\cdot\text{s}^{-1}$) at potential window from 0 to 1.6 V. The ASC possesses a specific capacitance of $113.48 \text{ F}\cdot\text{g}^{-1}$ at $5 \text{ mV}\cdot\text{s}^{-1}$ and the rectangularity of CV curves is slightly distorted due to the combination of double-layer capacitance of rGO and pseudocapacitance of PEDOT. The specific capacitance obtained from PVA/PEDOT nanofibers//rGO is higher than those of ASC-carbon fiber composites [36,37]. Figure 5b shows that the capacitance decreased gradually when the scan rates increased due to the reduced accessibility of electrolyte ions to fully diffused the interior surface of electrodes during the redox process [10]. Figure 5c indicates the CV curves of as-prepared PVA/PEDOT nanofibers//rGO asymmetric supercapacitor at a different operating potential (1.0 to 1.6 V) at a sweeping rate of $25 \text{ mV}\cdot\text{s}^{-1}$. Based on this result, the asymmetric composite obtained works stably until 1.6 V with nearly rectangular CV shape [11]. However, extending potential more than 2.0 V causes an obvious redox peak which leads to oxygen evolution [38].

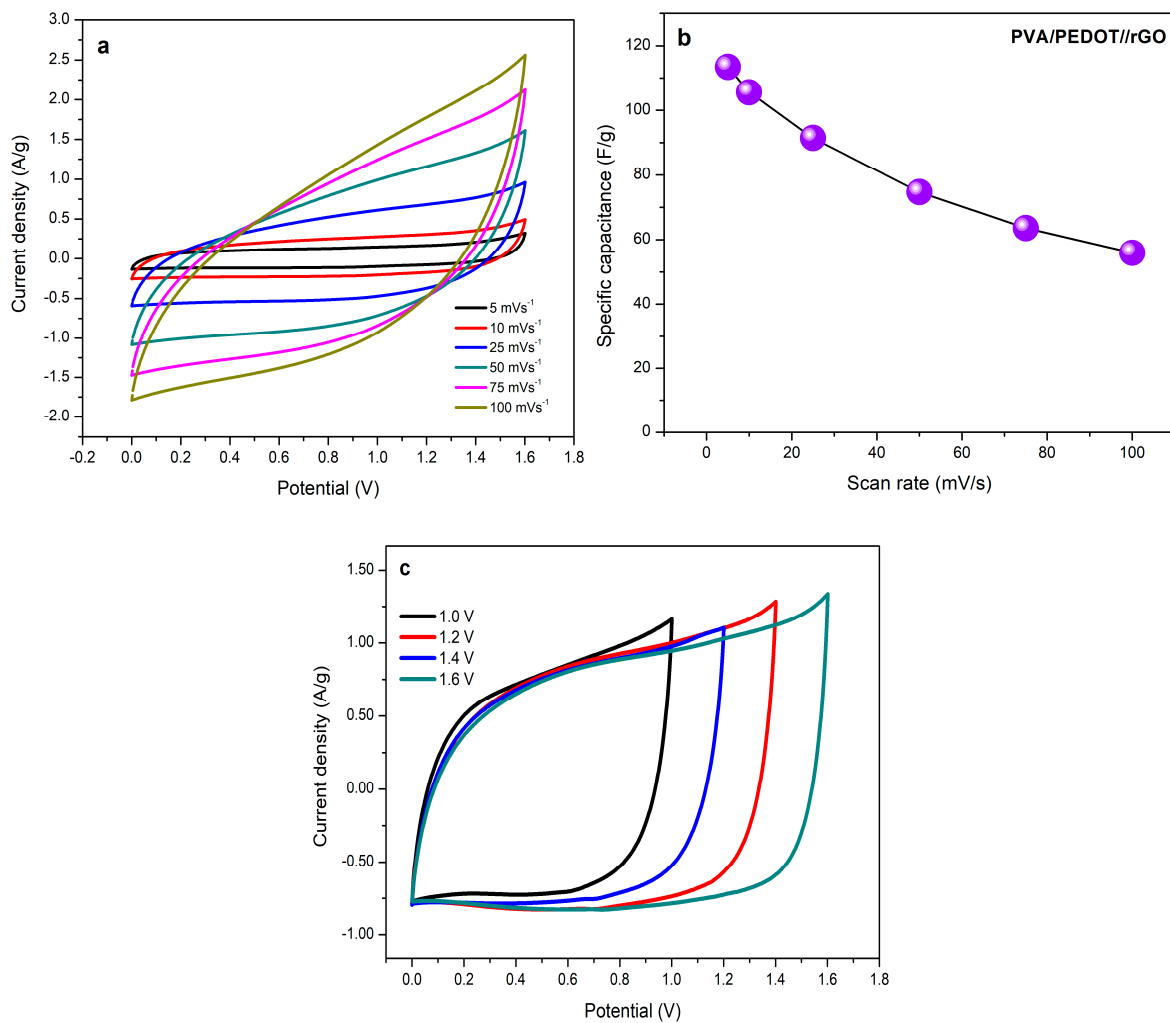


Figure 5. (a) CV curves of PVA/PEDOT nanofibers//rGO asymmetric cell at various sweeping rates ranging from 5 to 100 $\text{mV}\cdot\text{s}^{-1}$, (b) specific capacitance of PVA/PEDOT nanofibers//rGO cells at different sweeping rates, (c) CV profiles at potential windows from 1.0–1.6 V at sweeping rate of 25 $\text{mV}\cdot\text{s}^{-1}$.

The performance of the assembled ASC is further evaluated by GCD analysis at current densities from 0.4 to 0.8 $\text{A}\cdot\text{g}^{-1}$ at 1.6 V operating potential as shown in Figure 6a. PVA/PEDOT nanofibers//rGO shows a nearly symmetric triangular shape, showing an ideal capacitive behavior of PVA/PEDOT nanofibers//rGO [33]. A slight IR drop is observed at the beginning of these discharging curve, illustrating the influence of the internal resistance of electrode [39]. The ASC device displays equivalent series resistance (ESR) of about 33.33 Ω at a current density of 0.4 $\text{A}\cdot\text{g}^{-1}$. However, the initial voltage drops are small at higher current densities, implying small internal resistance of the asymmetric device [10]. As a result, the PVA/PEDOT nanofibers//rGO composite can achieve a total potential of 1.6 V at high current density, in agreement with a potential window of CV. The specific energy and specific power of ASC are obtained based on these equations [8]:

$$E = \frac{1}{2}C \times \Delta V^2 \quad (5)$$

$$P = \frac{E}{\Delta t}, \quad (6)$$

where E represents the specific energy ($\text{Wh}\cdot\text{kg}^{-1}$), P indicates the specific power ($\text{W}\cdot\text{kg}^{-1}$), C refers to the specific capacitance ($\text{F}\cdot\text{g}^{-1}$), Δt is the discharge time (h) and ΔV is the potential (V). Ragone plot (Figure 6b) of ASC PVA/PEDOT//rGO can deliver reasonably high specific energy of 21.25 $\text{Wh}\cdot\text{kg}^{-1}$ at

a specific power of $335.51 \text{ W}\cdot\text{kg}^{-1}$. Interestingly, the superior specific energy of ASC surpasses other PEDOT-based electrodes [4,27,40–42]. This remarkable supercapacitor behavior is due to the high specific capacitance obtained from the discharged time and extended potential window [43].

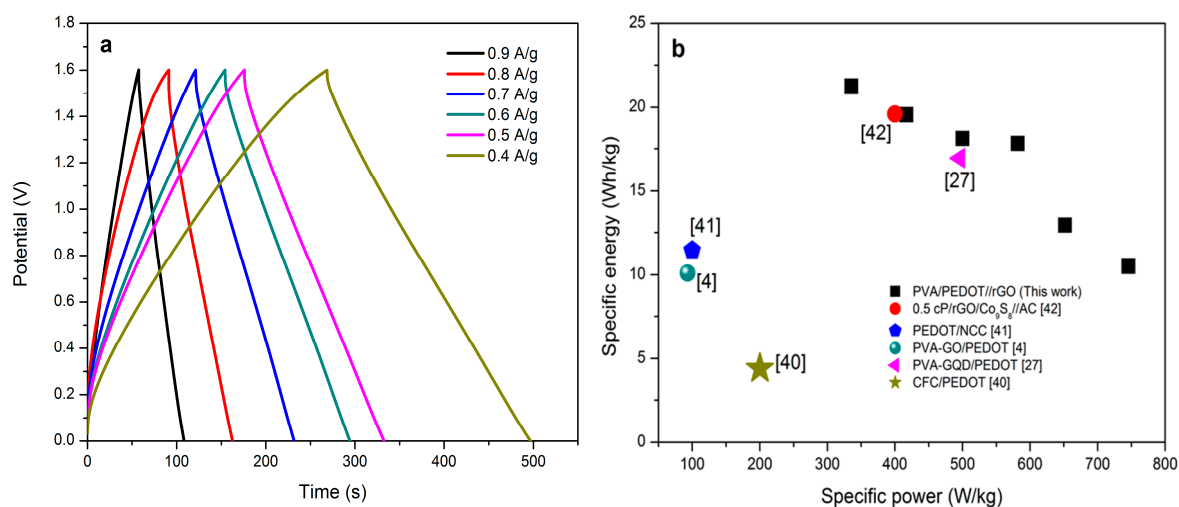


Figure 6. (a) Galvanostatic charge-discharge (GCD) curves at different current densities of PVA/PEDOT nanofibers//rGO. (b) Ragone plot of the asymmetric supercapacitor.

EIS measurements were performed to study the charge-transfer resistance (R_{ct}) and ESR of PVA/PEDOT nanofibers//rGO ASC (0.01 Hz to 100 kHz) as shown in Figure 7. From the Nyquist plot, two major parts can be identified. At the high-frequency region, the semicircle arc corresponds to the R_{ct} , where transport of ions at the electrode/electrolyte interface take place [33]. ESR comprises of intrinsic resistance of the electrode, ionic resistance of electrolyte and contact resistance at electrode/current collector [14]. The ESR is obtained from the x-intercept on the real axis (Z') at the high-frequency region. It is observed that the values for R_{ct} and ESR of ASC are 13.10Ω and 37.81Ω , respectively. Furthermore, the presence of a nearly vertical line along the imaginary axis in the low-frequency region suggests the good capacitive behaviors of the electrode [44]. The equivalent circuit fitting based on the Nyquist plot of PVA/PEDOT nanofibers//rGO ASC is shown in the inset of Figure 7. R_s represents the solution resistance, R_{ct} is charge transfer resistance and W is the Warburg impedance that related to the ionic diffusion. Constant phase element (CPE) was used to replace double layer capacitance due to the inhomogeneity and porous structure of the electrode surface [45].

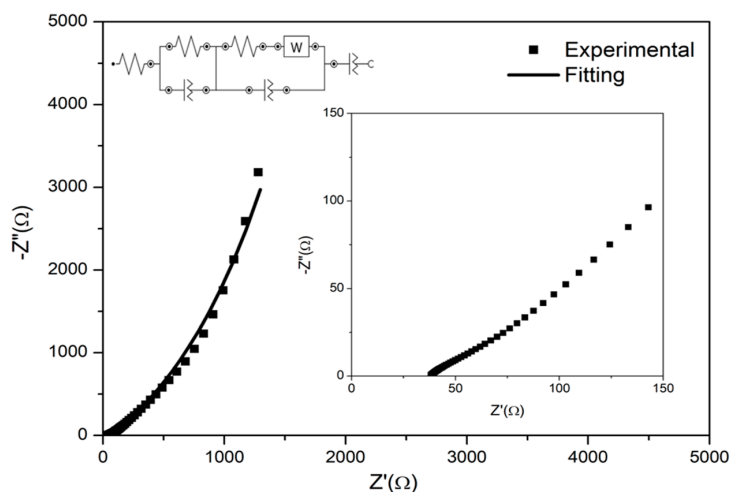


Figure 7. Nyquist plot of PVA/PEDOT nanofibers//rGO with an equivalent circuit.

The cycling stability of the asymmetric PVA/PEDOT nanofibers//rGO supercapacitor was investigated at $100 \text{ mV}\cdot\text{s}^{-1}$ for 5000 cycles. From Figure 8, the ASC presents excellent cycling stability by maintaining 83% of the initial capacitance after 5000 cycles. It is noted that a small increase of specific capacitance at cycle 600 is due to the improved wettability of PVA/PEDOT nanofibers//rGO [46] and high favorable of ions diffusion into the electrode surface [47]. As the cycle number continued, the capacitance decayed slightly with considerable retention, representing good cycling durability. The rGO as a negative electrode primarily provides high mechanical strength for the excellent cycling stability of the supercapacitor [48].

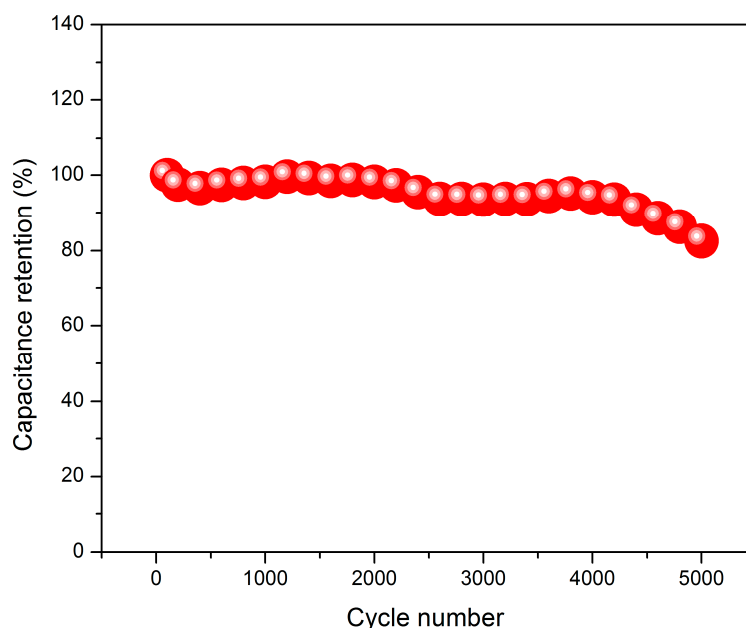


Figure 8. Cycling stability of PVA/PEDOT nanofibers//rGO asymmetric supercapacitor.

4. Conclusions

In conclusion, an ASC of PVA/PEDOT//rGO was successfully prepared using facile electrospinning and electrodeposition techniques. The PVA nanofibers provide a large surface area, enhancing more ion migration of electrolyte onto the electrode surface, resulting to a better specific capacitance at the maximum potential window of 1.6 V. A wrinkled morphology of rGO contributes good mechanical strength of ASC for high cycling stability over 5000 cycles. Interestingly, the synergistic effects of both electrodes illustrate remarkable specific energy ($21.25 \text{ Wh}\cdot\text{kg}^{-1}$) at $0.4 \text{ A}\cdot\text{g}^{-1}$. Therefore, these favorable capacitive performances of PVA/PEDOT//rGO can be served as a highly potential ASC electrode for future development supercapacitor application.

Author Contributions: N.D. performed the experiment and wrote the original draft. M.A.A.M.A. reviewed and edited the manuscript. Y.S. supervised the work and edited the manuscript.

Funding: This research was funded by the Universiti Putra Malaysia Research Grant (GP-IPS/2018/9619300).

Acknowledgments: The authors thanks for the characterization facilities provided by Universiti Putra Malaysia.

Conflicts of Interest: The authors declare no conflict of interest.

References

1. Rajkumar, M.; Hsu, C.-T.; Wu, T.-H.; Chen, M.-G.; Hu, C.-C. Advanced materials for aqueous supercapacitors in the asymmetric design. *Prog. Nat. Sci.-Mater. Int.* **2015**, *25*, 527–544. [[CrossRef](#)]
2. Kumar, M.; Subramania, A.; Balakrishnan, K. Preparation of electrospun Co_3O_4 nanofibers as electrode material for high performance asymmetric supercapacitors. *Electrochim. Acta* **2014**, *149*, 152–158. [[CrossRef](#)]

3. Hadjipaschalis, I.; Poullikkas, A.; Efthimiou, V. Overview of current and future energy storage technologies for electric power applications. *Renew. Sustain. Energy Rev.* **2009**, *13*, 1513–1522. [[CrossRef](#)]
4. Mohd Abdah, M.A.A.; Zubair, N.A.; Azman, N.H.N.; Sulaiman, Y. Fabrication of PEDOT coated PVA-GO nanofiber for supercapacitor. *Mater. Chem. Phys.* **2017**, *192*, 161–169. [[CrossRef](#)]
5. Kiran, S.K.; Padmini, M.; Das, H.T.; Elumalai, P. Performance of asymmetric supercapacitor using CoCr-layered double hydroxide and reduced graphene-oxide. *J. Solid State Electrochem.* **2017**, *21*, 927–938. [[CrossRef](#)]
6. Kumar, A.; Sanger, A.; Kumar, A.; Kumar, Y.; Chandra, R. An efficient α -MnO₂ nanorods forests electrode for electrochemical capacitors with neutral aqueous electrolytes. *Electrochim. Acta* **2016**, *220*, 712–720. [[CrossRef](#)]
7. Mohammadi, A.; Arsalani, N.; Tabrizi, A.G.; Moosavifard, S.E.; Naqshbandi, Z.; Ghadimi, L.S. Engineering rGO-CNT wrapped Co₃S₄ nanocomposites for high-performance asymmetric supercapacitors. *Chem. Eng. J.* **2018**, *334*, 66–80. [[CrossRef](#)]
8. Ning, P.; Duan, X.; Ju, X.; Lin, X.; Tong, X.; Pan, X.; Wang, T.; Li, Q. Facile synthesis of carbon nanofibers/MnO₂ nanosheets as high-performance electrodes for asymmetric supercapacitors. *Electrochim. Acta* **2016**, *210*, 754–761. [[CrossRef](#)]
9. Bhagwan, J.; Sivasankaran, V.; Yadav, K.L.; Sharma, Y. Porous, one-dimensional and high aspect ratio nanofibric network of cobalt manganese oxide as a high performance material for aqueous and solid-state supercapacitor (2 V). *J. Power Sources* **2016**, *327*, 29–37. [[CrossRef](#)]
10. Wang, J.-G.; Yang, Y.; Huang, Z.-H.; Kang, F. A high-performance asymmetric supercapacitor based on carbon and carbon-MnO₂ nanofiber electrodes. *Carbon* **2013**, *61*, 190–199. [[CrossRef](#)]
11. Peng, H.; Ma, G.; Sun, K.; Mu, J.; Luo, M.; Lei, Z. High-performance aqueous asymmetric supercapacitor based on carbon nanofibers network and tungsten trioxide nanorod bundles electrodes. *Electrochim. Acta* **2014**, *147*, 54–61. [[CrossRef](#)]
12. Zhang, C.; Wei, J.; Chen, L.; Tang, S.; Deng, M.; Du, Y. All-solid-state asymmetric supercapacitors based on Fe-doped mesoporous Co₃O₄ and three-dimensional reduced graphene oxide electrodes with high energy and power densities. *Nanoscale* **2017**, *9*, 15423–15433. [[CrossRef](#)] [[PubMed](#)]
13. Chen, Q.; Cai, D.; Zhan, H. Construction of reduced graphene oxide nanofibers and cobalt sulfide nanocomposite for pseudocapacitors with enhanced performance. *J. Alloys Compd.* **2017**, *706*, 126–132. [[CrossRef](#)]
14. Miniach, E.; Śliwak, A.; Moysowicz, A.; Fernández-García, L.; González, Z.; Granda, M.; Menendez, R.; Gryglewicz, G. MnO₂/thermally reduced graphene oxide composites for high-voltage asymmetric supercapacitors. *Electrochim. Acta* **2017**, *240*, 53–62. [[CrossRef](#)]
15. Jiang, L.; Sui, Y.; Qi, J.; Chang, Y.; He, Y.; Meng, Q.; Wei, F.; Sun, Z.; Jin, Y. Hierarchical Ni-Co layered double hydroxide nanosheets on functionalized 3D-RGO films for high energy density asymmetric supercapacitor. *Appl. Surf. Sci.* **2017**, *426*, 148–159. [[CrossRef](#)]
16. Lamiel, C.; Lee, Y.R.; Cho, M.H.; Tuma, D.; Shim, J.-J. Enhanced electrochemical performance of nickel-cobalt-oxide@reduced graphene oxide/activated carbon asymmetric supercapacitors by the addition of a redox-active electrolyte. *J. Colloid Interface Sci.* **2017**, *507*, 300–309. [[CrossRef](#)] [[PubMed](#)]
17. Huang, L.; Liu, B.; Hou, H.; Wu, L.; Zhu, X.; Hu, J.; Yang, J. Facile preparation of flower-like NiMn layered double hydroxide/reduced graphene oxide microsphere composite for high-performance asymmetric supercapacitors. *J. Alloys Compd.* **2018**, *730*, 71–80. [[CrossRef](#)]
18. Mao, X.; Yang, W.; He, X.; Chen, Y.; Zhao, Y.; Zhou, Y.; Yang, Y.; Xu, J. The preparation and characteristic of poly (3,4-ethylenedioxythiophene)/reduced graphene oxide nanocomposite and its application for supercapacitor electrode. *Mater. Sci. Eng. B* **2017**, *216*, 16–22. [[CrossRef](#)]
19. Yang, H.; Xu, H.; Li, M.; Zhang, L.; Huang, Y.; Hu, X. Assembly of NiO/Ni(OH)₂/PEDOT Nanocomposites on Contra Wires for Fiber-Shaped Flexible Asymmetric Supercapacitors. *ACS Appl. Mater. Interfaces* **2016**, *8*, 1774–1779. [[CrossRef](#)]
20. Sun, K.; Zhang, S.; Li, P.; Xia, Y.; Zhang, X.; Du, D.; Isikgor, F.H.; Ouyang, J. Review on application of PEDOTs and PEDOT:PSS in energy conversion and storage devices. *J. Mater. Sci. Mater. Electron.* **2015**, *26*, 4438–4462. [[CrossRef](#)]
21. Shin, D.Y.; An, G.H.; Ahn, H.J. Barnacle-like manganese oxide decorated porous carbon nanofibers for high-performance asymmetric supercapacitors. *Ceram. Int.* **2018**, *44*, 4883–4890. [[CrossRef](#)]

22. Liu, Y.; Zhou, J.; Fu, W.; Zhang, P.; Pan, X.; Xie, E. In situ synthesis of CoS_x@carbon core-shell nanospheres decorated in carbon nanofibers for capacitor electrodes with superior rate and cycling performances. *Carbon* **2017**, *114*, 187–197. [[CrossRef](#)]
23. Zhao, P.; Yao, M.; Ren, H.; Wang, N.; Komarneni, S. Nanocomposites of hierarchical ultrathin MnO₂ nanosheets/hollow carbon nanofibers for high-performance asymmetric supercapacitors. *Appl. Surf. Sci.* **2019**, *463*, 931–938. [[CrossRef](#)]
24. Zubair, N.A.; Rahman, N.A.; Lim, H.N.; Sulaiman, Y. Production of Conductive PEDOT-Coated PVA-GO Composite Nanofibers. *Nanoscale Res. Lett.* **2017**, *12*, 113. [[CrossRef](#)] [[PubMed](#)]
25. Zhao, X.; Zhang, Q.; Chen, D.; Lu, P. Enhanced Mechanical Properties of Graphene-Based Poly(vinyl alcohol) Composites. *Macromolecules* **2010**, *43*, 2357–2363. [[CrossRef](#)]
26. Pan, Q.; Tong, N.; He, N.; Liu, Y.; Shim, E.; Pourdeyhimi, B.; Gao, W. Electrospun Mat of Poly(vinyl alcohol)/Graphene Oxide for Superior Electrolyte Performance. *ACS Appl. Mater. Interfaces* **2018**, *10*, 7927–7934. [[CrossRef](#)] [[PubMed](#)]
27. Syed Zainol Abidin, S.N.J.; Mamat, S.; Abdul Rasyid, S.; Zainal, Z.; Sulaiman, Y. Fabrication of poly(vinyl alcohol)-graphene quantum dots coated with poly(3,4-ethylenedioxythiophene) for supercapacitor. *J. Polym. Sci. A* **2017**, *56*, 50–58. [[CrossRef](#)]
28. Oh, Y.J.; Yoo, J.J.; Kim, Y.I.; Yoon, J.K.; Yoon, H.N.; Kim, J.-H.; Park, S.B. Oxygen functional groups and electrochemical capacitive behavior of incompletely reduced graphene oxides as a thin-film electrode of supercapacitor. *Electrochim. Acta* **2014**, *116*, 118–128. [[CrossRef](#)]
29. Yohannes, T.; Carlberg, J.C.; Inganäs, O.; Solomon, T. Electrochemical and spectroscopic characteristics of copolymers electrochemically synthesized from 3-methylthiophene and 3,4-ethylenedioxy thiophene. *Synth. Met.* **1997**, *88*, 15–21. [[CrossRef](#)]
30. Ma, Y.; Zhao, F.; Zeng, B. Electrodeposition of poly(3,4-ethylenedioxythiophene) on a stainless steel wire for solid phase microextraction and GC determination of some esters with high boiling points. *Talanta* **2013**, *104*, 27–31. [[CrossRef](#)]
31. Bonanni, A.; Ambrosi, A.; Pumera, M. On oxygen-containing groups in chemically modified graphenes. *Chem. Eur. J.* **2012**, *18*, 4541–4548. [[CrossRef](#)] [[PubMed](#)]
32. Doğan, H.Ö.; Ekinçi, D.; Demir, Ü. Atomic scale imaging and spectroscopic characterization of electrochemically reduced graphene oxide. *Surf. Sci* **2013**, *611*, 54–59. [[CrossRef](#)]
33. Lin, S.-C.; Lu, Y.-T.; Chien, Y.-A.; Wang, J.-A.; You, T.-H.; Wang, Y.-S.; Lin, C.-W.; Ma, C.-C.M.; Hu, C.-C. Asymmetric supercapacitors based on functional electrospun carbon nanofiber/manganese oxide electrodes with high power density and energy density. *J. Power Sources* **2017**, *362*, 258–269. [[CrossRef](#)]
34. Cai, J.; Niu, H.; Wang, H.; Shao, H.; Fang, J.; He, J.; Xiong, H.; Ma, C.; Lin, T. High-performance supercapacitor electrode from cellulose-derived, inter-bonded carbon nanofibers. *J. Power Sources* **2016**, *324*, 302–308. [[CrossRef](#)]
35. Shivakumara, S.; Munichandraiah, N. Asymmetric supercapacitor based on nanostructured porous manganese oxide and reduced graphene oxide in aqueous neutral electrolyte. *Solid State Commun.* **2017**, *260*, 34–39. [[CrossRef](#)]
36. Cho, S.; Patil, B.; Yu, S.; Ahn, S.; Hwang, J.; Park, C.; Do, K.; Ahn, H. Flexible, Swiss roll, fiber-shaped, asymmetric supercapacitor using MnO₂ and Fe₂O₃ on carbon fibers. *Electrochim. Acta* **2018**, *269*, 499–508.
37. Ye, A.; Sui, Y.; Qi, J.; Wei, F.; He, Y.; Meng, Q.; Ren, Y.; Sun, Z. Self-Supported Ni_{0.85}Se Nanosheets Array on Carbon Fiber Cloth for a High-Performance Asymmetric Supercapacitor. *J. Electron. Mater.* **2018**, *47*, 7002–7010. [[CrossRef](#)]
38. Lv, Y.; Wang, H.; Xu, X.; Shi, J.; Liu, W.; Wang, X. Balanced mesoporous nickel cobaltite-graphene and doped carbon electrodes for high-performance asymmetric supercapacitor. *Chem. Eng. J.* **2017**, *326*, 401–410. [[CrossRef](#)]
39. Zhou, Z.; Wu, X.-F. Graphene-beaded carbon nanofibers for use in supercapacitor electrodes: Synthesis and electrochemical characterization. *J. Power Sources* **2013**, *222*, 410–416. [[CrossRef](#)]
40. Rajesh, M.; Raj, J.; Manikandan, R.; Kim, B.C.; Yeup Park, S.; Hyun Yu, K. A High Performance PEDOT/PEDOT Symmetric Supercapacitor by Facile in-situ Hydrothermal Polymerization of PEDOT Nanostructures on Flexible Carbon Fibre Cloth Electrodes. *Mater. Today Energy* **2017**, *6*, 96–104. [[CrossRef](#)]

41. Ravit, R.; Abdullah, J.; Ahmad, I.; Sulaiman, Y. Electrochemical performance of poly(3,4-ethylenedioxythiophene)/nanocrystalline cellulose (PEDOT/NCC) film for supercapacitor. *Carbohydr. Polym.* **2019**, *203*, 128–138. [[CrossRef](#)] [[PubMed](#)]
42. Yao, T.; Li, Y.; Liu, D.; Gu, Y.; Qin, S.; Guo, X.; Guo, H.; Ding, Y.; Liu, Q.; Chen, Q.; et al. High-performance free-standing capacitor electrodes of multilayered Co₉S₈ plates wrapped by carbonized poly(3,4-ethylenedioxythiophene):poly(styrene sulfonate)/reduced graphene oxide. *J. Power Sources* **2018**, *379*, 167–173. [[CrossRef](#)]
43. Pan, Y.; Gao, H.; Zhang, M.; Li, L.; Wang, G.; Shan, X. Three-dimensional porous ZnCo₂O₄ sheet array coated with Ni(OH)₂ for high-performance asymmetric supercapacitor. *J. Colloid Interface Sci.* **2017**, *497*, 50–56. [[CrossRef](#)] [[PubMed](#)]
44. Feng, L.; Li, G.; Zhang, S.; Zhang, Y.X. Decoration of carbon cloth by manganese oxides for flexible asymmetric supercapacitors. *Ceram. Int.* **2017**, *43*, 8321–8328. [[CrossRef](#)]
45. Xiao, F.; Xu, Y. Pulse Electrodeposition of Manganese Oxide for High-Rate Capability Supercapacitors. *Int. J. Electrochem. Sci.* **2012**, *7*, 7440–7450.
46. Huang, Y.; Shi, T.; Jiang, S.; Cheng, S.; Tao, X.; Zhong, Y.; Liao, G.; Tang, Z. Enhanced cycling stability of NiCo₂S₄@NiO core-shell nanowire arrays for all-solid-state asymmetric supercapacitors. *Sci. Rep.* **2016**, *6*, 38620. [[CrossRef](#)]
47. Zhou, J.; Lian, J.; Hou, L.; Zhang, J.; Gou, H.; Xia, M.; Zhao, Y.; Strobel, T.A.; Tao, L.; Gao, F. Ultrahigh volumetric capacitance and cyclic stability of fluorine and nitrogen co-doped carbon microspheres. *Nat. Commun.* **2015**, *6*, 8503. [[CrossRef](#)]
48. Li, Q.; Lu, C.; Chen, C.; Xie, L.; Liu, Y.; Li, Y.; Kong, Q.; Wang, H. Layered NiCo₂O₄/reduced graphene oxide composite as an advanced electrode for supercapacitor. *Energy Storage Mater.* **2017**, *8*, 59–67. [[CrossRef](#)]



© 2019 by the authors. Licensee MDPI, Basel, Switzerland. This article is an open access article distributed under the terms and conditions of the Creative Commons Attribution (CC BY) license (<http://creativecommons.org/licenses/by/4.0/>).